IEEE Access
Multidisciplinary | Rapid Review | Open Access Journal

Received July 8, 2019, accepted August 5, 2019, date of publication August 8, 2019, date of current version August 21, 2019.

Digital Object Identifier 10.1109/ACCESS.2019.2933897

Adaptive Bandwidth Fourier Decomposition Method for Multi-Component Signal Processing

MINQIANG DENG, AIDONG DENG, JING ZHU, AND WENQING SUN

National Engineering Research Center of Turbo-Generator Vibration, School of Energy and Environment, Southeast University, Nanjing 210096, China

Corresponding author: Aidong Deng (dnh@seu.edu.cn)

This work was supported by the National Natural Science Foundation of China under Grant 51875100.

ABSTRACT Variational mode decomposition (VMD) is a practical signal decomposition approach, which extracts the modes through bandwidth optimization in the frequency domain. In recent years, many efforts have been made to attenuate the effect of prior parameters, which heavily trouble the traditional VMD. However, as the core step, the bandwidth optimization algorithm including the initialization of center frequencies in VMD is rarely discussed or improved in the existing work. In practical applications, the non-convergence or unreasonable convergence of the bandwidth optimization can lead to the failure of VMD in mode separation. Thus, in this paper, a new signal decomposition method termed adaptive bandwidth Fourier decomposition (ABFD) is proposed to separate the narrowband components from a complicated signal accurately. The proposed ABFD inherits the idea of implementing Fourier spectrum decomposition through bandwidth optimization. In particular, three significant improvements are made in this work. Firstly, in order to reduce the computation complexity, a novel bandwidth optimization algorithm termed Fourier spectrum bandwidth optimization (FSBO) is proposed. Secondly, inspired by the empirical principle proposed in the empirical wavelet transform (EWT), a novel variable initialization method based on spectral energy distribution is introduced. Finally, under the guidance of narrowband characteristics, a method for automatically detecting the appropriate mode number is developed. In order to evaluate the performance of the proposed ABFD, simulation analysis and measured signal analysis are carried out in this paper. The preliminary results indicate that the proposed ABFD can extract the single components more accurately than EMD and VMD.

INDEX TERMS Signal processing, Fourier transform, signal analysis, signal decomposition, adaptive bandwidth Fourier decomposition, empirical mode decomposition (EMD), variational mode decomposition (VMD).

I. INTRODUCTION

There are a large number of unstable signals in nature, which usually contain important information. The commonly used Fourier transform (FT) is suitable for the analysis of linear and stationary data, but it does not effectively reveal the characteristics of time-varying signals [1]. Therefore, the processing of unstable signals has always been the focus of academic and engineering circles. The traditional methods including short-time Fourier transform (STFT), Wigner-Ville Distribution (WVD), and wavelet transform (WT), etc., are widely used in processing single-component chirp signals while their performance is not satisfactory when dealing with multi-component non-linear and non-stationary signals [2]. For instance, the STFT has a contradiction between time domain resolution and frequency domain resolution. In the multi-component signal analysis, the WVD is constrained by the interference of cross terms. The results obtained by WT depend on the manual selection of predefined wavelet basis and decomposition layers, which limits the application of wavelet transform.

In order to effectively mine and analyze the time-varying characteristics hidden in the complicated signals, signal decomposition technologies have been developed in recent years. In 1998, Huang [3] proposed an adaptive signal decomposition method for non-stationary signal analysis, namely

The associate editor coordinating the review of this article and approving it for publication was Zhen Ren.

empirical mode decomposition (EMD). The algorithm recursively removes the average of the upper and lower envelope to extract the high-frequency oscillation as the ''mode'' of the signal [4]. Undoubtedly, the construction of the envelope and the mean curve is a crucial step in EMD [5]. In recent years, many improvements have been made in the construction of the average curve and some new adaptive methods that maintain the global recursive sifting structure of EMD have been proposed [6]. Although EMD and its improved algorithms have achieved great success, they are all empirical, which makes their solutions lack the support of mathematical theory [7]. Besides, EMD is susceptible to modal aliasing and endpoint effects when processing the measured noisy signals [8]. In order to avoid the inherent defects of EMD, Gilles proposed a new signal decomposition method in 2013, namely the empirical wavelet transform (EWT) [9]. The EWT is developed to construct the appropriate orthogonal wavelet filter banks to separate the amplitude modulated-frequency modulated (AM-FM) components with compact Fourier spectrum. However, EWT is sensitive to the division of the Fourier spectrum, and the calculation results are susceptible to noise interference [10].

Recently, a new signal decomposition method called variational mode decomposition (VMD) is proposed by Dragomiretskiy [11]. VMD assumes that each mode closely surrounds a particular center frequency and transforms the mode decomposition into a variational solution problem. This method avoids the inherent defects of recursive decomposition and reflects several advantages, including reliable mathematical support, anti-noise and suppression mode aliasing [12]. Therefore, many successful applications of VMD technology have been reported in the past few years. For instance, Bi *et al.* took the fourth-order cumulant of restructured signals from VMD as fault indexes to detect multiple types of engine faults [13]. Wang *et al.* developed a weak degradation characteristic extraction method based on VMD and Laplacian Eigenmaps (LE) to identify the degradation information of brushless direct current (BLDC) motors [14]. Jiang *et al.* proposed a new VMD-based coarse-to-fine decomposing strategy to obtain the optimal mode and extract the weak repetitive transients of rotating machines [15]. However, the decomposition results of VMD depend on the reasonable predefinition of parameters, including the mode number K, the balance parameter α, the update parameter τ, and the convergence tolerance parameter ε [16]. Therefore, the selection of appropriate decomposition parameters has become a research focus in the application of VMD method. For instance, to accurately extract the rolling bearing fault features, Wei *et al.* used the envelope entropy as a fitness function of the whale optimization algorithm (WOA) to obtain the optimal parameters of the VMD method [17]. Li *et al.* proposed a variable dimension chaotic pigeon-inspired optimization (VDCPIO) algorithm to search for the optimal combination of key parameters of VMD [18]. To improve the online processing ability, the scale space segmentation method was introduced in [19] to determine the number K of the intrinsic mode functions (IMFs) decomposed by VMD. Based on the characteristics of IMF, Lian *et al.* proposed a method called Adaptive Variational Mode Decomposition (AVMD) to determine the mode number automatically. This method judges the VMD's decomposition results in the guide of a series of indicators, including permutation entropy, extreme value in the frequency domain, kurtosis criterion, and energy loss coefficient, etc. [20]

According to the literature review, many studies have focused on optimizing the decomposition parameters to reduce the impact of the prior parameters. However, the improved VMD method still has some problems to be solved when applied to the multi-component signals. Firstly, in the improved VMD method, the parameter optimization strategy defined for a particular application does not necessarily apply to all scenarios. In addition, parameter optimization is an iterative optimization process, which consumes a large number of computing resources. Thus, the adaptability of VMD needs to be further improved. Secondly, the core step of VMD is the bandwidth optimization through alternate direction method of multipliers (ADMM), which is essentially an iterative calculation method. Considering the influence of initialization on the convergence of iterative calculation, the initial center frequencies can significantly affect the decomposing efficiencies and analysis results [21]. However, this problem is rarely discussed or reported in the available literature. Besides, although the VMD algorithm is developed on the basis of strict mathematical theory, the final decomposition results are not necessarily deterministic or interpretable, because the convergence of iterative calculation for bandwidth optimization cannot be guaranteed in the VMD method. Undoubtedly, non-convergence or unreasonable convergence can lead to the failure of signal separation and the loss of valuable information, which will be demonstrated in the simulation analysis of this paper. Therefore, the bandwidth optimization algorithm including the variable initialization strategy needs to be further investigated and improved.

Motivated by the merits and shortcomings of VMD, a new signal decomposition method termed ABFD is proposed in this paper to extract the narrowband components more accurately. The proposed ABFD is developed to decompose the signal into a series of narrowband sub-signals in the frequency domain through bandwidth optimization. In order to avoid the drawbacks of VMD mentioned above, some improvements have been made to enhance the performance of signal decomposition. Firstly, to reduce the computational complexity, a novel bandwidth optimization algorithm termed Fourier spectrum bandwidth optimization (FSBO) is proposed based on energy distribution in the frequency domain. The analysis results demonstrate that compared with VMD, the proposed FSBO algorithm improves the convergence speed and stability of iterative calculation. Then, considering the influence of initialization on the iterative calculation, a novel variable initialization method based on the spectral energy distribution is developed to better separate the individual components from the mixed signal. After that,

a method for automatically determining the mode number is proposed on the basis of narrowband characteristics of mono-component signals. Therefore, compared with VMD and its improved algorithms, the proposed ABFD makes full use of the features of spectral energy distribution to improve its performance. To verify the validity of the proposed ABFD method, three typical simulation signal analyses are introduced in this paper, including decomposition capability analysis, non-stationary signal analysis, and noisy signal analysis. Furthermore, two measured vibration signals are utilized to evaluate the performance of ABFD in practical applications. The preliminary results show that compared with EMD and VMD, the proposed ABFD can better separate the narrowband components in different application scenarios.

The rest of this paper is organized as follows. In Section II, the principle of ABFD is discussed in detail. After that, the ABFD is employed to conduct the simulation signal analysis in Section III. Meanwhile, the results are compared to the ones obtained by EMD and VMD. Section IV mainly analyzes the decomposition results of measured vibration signals. In section V, the computational efficiency is discussed. Finally, some conclusions are drawn in Section VI.

II. ADAPTIVE BANDWIDTH FOURIER DECOMPOSITION

In this section, the principle of ABFD is described in detail.

Inspired by VMD, the goal of ABFD is to adaptively decompose the original signal $f(t)$ into a series of individual sub-signals $\{U_k(\omega)\}$ in the frequency domain through bandwidth optimization. According to the definition of mode in VMD, the separated sub-signals are expected to have a compact Fourier spectrum. Then, the sub-signals in the frequency domain are converted into time-domain signals named bandwidth mode function (BMF) through inverse Fourier transform. As mentioned in Section I, the main improvements of ABFD include three parts: 1) a novel bandwidth optimization algorithm named FSBO; 2) an improved variable initialization strategy; 3) automatic detection for the number of BMFs. Therefore, the theoretical principles of ABFD will be demonstrated from these three aspects.

A. FOURIER SPECTRUM BANDWIDTH OPTIMIZATION

To begin with, we assume that the mode number K is given. In order to optimize the bandwidth of all modes, a practical bandwidth estimation method is required. In the conventional VMD algorithm, the bandwidth of a mode is evaluated through the Gaussian smoothness of the demodulated signal, which leads to complex iterative calculations. Therefore, a new bandwidth estimation method based on the energy distribution in the frequency domain is introduced in this paper [22].

$$B = \int_{-\infty}^{+\infty} |U_k(\omega)|^2 (\omega - \omega_k)^2 d\omega \tag{1}$$

where B stands for the bandwidth estimation of sub-signal $U_k(\omega)$ and ω_k is its center frequency. Considering the symmetry of the Fourier spectrum of the real signal, it is defined that in the ABFD method, the frequency domain signals such as $F(\omega)$ and $U_k(\omega)$ take the unilateral Fourier spectrum. Furthermore, to reduce the computational complexity, we define that the frequency domain signals $\{U_k(\omega)\}$ have the same phase angle as $F(\omega)$:

$$U_k(\omega) = \frac{|U_k(\omega)|}{|F(\omega)|} \cdot F(\omega), \quad k = 1, 2, \ldots K \tag{2}$$

where $F(\omega)$ represents the Fourier spectrum of the input signal $f(t)$. Then, the resulting constrained problem $L_0(\{U_k(\omega)\}, \{\omega_k\})$ of bandwidth optimization is constructed as follows:

$$\begin{aligned} &L_0(\{U_k(\omega)\}, \{\omega_k\}) \\ &= \min_{\{u_k\},\{\omega_k\}} \left\{ \sum_K \int_{-\infty}^{+\infty} |U_k(\omega)(\omega - \omega_k)|^2 d\omega \right\} \\ &\quad s.t. \begin{cases} \sum_K |U_k(\omega)| = |F(\omega)| \\ |U_k(\omega)| \geq 0 \end{cases} \end{aligned} \tag{3}$$

Constrained optimization problems can be solved in many different ways. In this paper, in order to obtain the deterministic analytical solution, the problem in Eq. (3) is transformed into the unconstrained optimization problem $L_1(\{U_k(\omega)\}, \{\omega_k\})$ through the Lagrange multiplier method:

$$\begin{aligned} &L_1(\{U_k(\omega)\}, \{\omega_k\}) \\ &= \min_{\{U_k(\omega)\},\{\omega_k\}} \left\{ \begin{aligned} &\sum_K \int_{-\infty}^{+\infty} |U_k(\omega)(\omega - \omega_k)|^2 d\omega \\ &+ \int_{-\infty}^{+\infty} \lambda(\omega) \cdot (|F(\omega)| - \sum_K |U_k(\omega)|) d\omega \end{aligned} \right\} \end{aligned} \tag{4}$$

where $\lambda(\omega)$ denotes the Lagrange multiplier. Then, Eq. (4) is transformed into a more easily solved Eq. (5).

$$\begin{aligned} &L_1(\{U_k(\omega)\}, \{\omega_k\}) \\ &= \min_{\{U_k(\omega)\},\{\omega_k\}} \left\{ \int_{-\infty}^{+\infty} \left[\begin{aligned} &\sum_K |U_k(\omega)|^2 \cdot (\omega - \omega_k)^2 \\ &+ \lambda(\omega) \cdot (|F(\omega)| - \sum_K |U_k(\omega)|) \end{aligned} \right] d\omega \right\} \end{aligned} \tag{5}$$

At the saddle points of the quadratic optimization problem, the objective function $L_1(\{U_k(\omega)\}, \{\omega_k\})$ takes the minimum value, that is, the bandwidth optimization problem can be solved by finding the saddle points of Eq. (5). At saddle points, the partial derivatives of $L_1(\{U_k(\omega)\}, \{\omega_k\})$ to $|U_k(\omega)|$, $\lambda(\omega)$ and ω_k are all equal to zero, as shown below:

$$\frac{\partial L_1}{\partial |U_k(\omega)|} = 2|U_k(\omega)|(\omega - \omega_k)^2 - \lambda(\omega) = 0, \quad k = 1, 2, \ldots K \tag{6}$$

$$\frac{\partial L_1}{\partial \lambda(\omega)} = |F(\omega)| - \sum_K |U_k(\omega)| = 0 \tag{7}$$

$$\frac{\partial L_1}{\partial \omega_k} = 2 \int_{-\infty}^{+\infty} |U_k(\omega)|^2 (\omega - \omega_k) d\omega = 0, \quad k = 1, 2, \ldots K \tag{8}$$

where L_1 is the objective function in Eq. (5). It can be observed that Eq. (6) and Eq. (7) are linear equations if ω_k is temporarily taken as a constant. Then, the analytical solutions of $|U_k(\omega)|$ and $\lambda(\omega)$ can be easily obtained by solving Eq. (6) and Eq. (7) simultaneously, as shown in Eq. (9) and Eq. (10).

$$|U_k(\omega)| = \begin{cases} \dfrac{|F(\omega)|}{(\omega-\omega_k)^2 \sum\limits_K \frac{1}{(\omega-\omega_k)^2}}, & \omega \notin \{\omega_k\} \\ 0, & \omega = \omega_{i,i\neq k} \\ |F(\omega)|, & \omega = \omega_k \end{cases} \tag{9}$$

$$\lambda(\omega) = \begin{cases} \dfrac{2\,|F(\omega)|}{\sum\limits_K \frac{1}{(\omega-\omega_k)^2}}, & \omega \notin \{\omega_k\} \\ 0, & \omega \in \{\omega_k\} \end{cases} \tag{10}$$

After that, submitting the Eq. (15) into Eq. (9) yields the analytical solution of $U_k(\omega)$, expressed as:

$$U_k(\omega) = \begin{cases} \dfrac{F(\omega)}{(\omega-\omega_k)^2 \sum\limits_K \frac{1}{(\omega-\omega_k)^2}}, & \omega \notin \{\omega_k\} \\ 0, & \omega = \omega_{i,i\neq k} \\ F(\omega), & \omega = \omega_k \end{cases} \tag{11}$$

As can be seen, the Eq. (11) is explicit, that is, in the case where $\{\omega_k\}$ is determined, $U_k(\omega)$ can be obtained directly. Therefore, the complicated bandwidth optimization problem is equivalent to searching the appropriate center frequencies, which effectively reduces the computational complexity. According to Eq. (8), the center frequency ω_k is easily solved as:

$$\omega_k = \frac{\int_{-\infty}^{+\infty} \omega\,|U_k(\omega)|^2\,d\omega}{\int_{-\infty}^{+\infty} |U_k(\omega)|^2\,d\omega} \tag{12}$$

It can be seen from Eq. (12) that the solution of ω_k is implicit and can be solved by the iterative calculation shown in Eq. (13).

$$\omega_k^{n+1} = \frac{\int_{-\infty}^{+\infty} \omega\,\left|U_k^n(\omega)\right|^2\,d\omega}{\int_{-\infty}^{+\infty} \left|U_k^n(\omega)\right|^2\,d\omega} \tag{13}$$

where ω_k^{n+1} is the update of ω_k^n; U_k^{n+1} represents the update of U_k^n. After the iteration of Eq. (13) converges, the final $U_k^{n+1}(\omega)$ will be taken as the solution of bandwidth optimization, that is, the Fourier spectrum of BMF.

For a better understanding, the complete bandwidth optimization algorithm that decomposes the $F(\omega)$ to $\{U_k(\omega)\}$ is summarized as follows.

The parameter ε is the criterion for convergence judgment, which tends to zero. In this paper, ε takes 0.001.

Algorithm 1 Fourier Spectrum Bandwidth Optimization

Input: $F(\omega)$, mode number K
Output: $\{U_k(\omega)\}$
Begin
n $\leftarrow$ 0
$\{\omega_k\}$ initialization
repeat
n $\leftarrow$ n + 1
for $k = 1{:}\,K$ do

$$U_k^n(\omega) = \begin{cases} \dfrac{F(\omega)}{\left(\omega-\omega_k^n\right)^2 \sum\limits_K \frac{1}{(\omega-\omega_k^n)^2}}, & \omega \notin \left\{\omega_k^n\right\} \\ 0, & \omega = \omega_{i,i\neq k}^n \\ F(\omega), & \omega = \omega_k^n \end{cases} \tag{14}$$

$$\omega_k^{n+1} = \frac{\int_{-\infty}^{+\infty} \omega\,\left|U_k^n(\omega)\right|^2\,d\omega}{\int_{-\infty}^{+\infty} \left|U_k^n(\omega)\right|^2\,d\omega} \tag{15}$$

end for
until convergence: $\max\left|\left(\omega_k^{n+1}-\omega_k^n\right)\right| < \varepsilon$
End

B. INITIALIZATION OF CENTER FREQUENCIES

From the previous analysis, the initialization of variables has an important impact on the iterative calculation. In the VMD method, it is recommended to initialize the center frequencies in the unilateral Fourier spectrum uniformly. This initialization method ignores the characteristics of the Fourier spectrum and may lead to unreasonable convergence in practical applications. Therefore, to improve the convergence speed and accuracy, an improved variable initialization method is proposed in this paper.

The goal of signal decomposition is to separate the narrowband AM-FM components from the mixed signal accurately. In [9], an empirical principle is proposed in which the center frequency point of the Fourier spectrum corresponding to the desired narrowband AM-FM component is a significant maximum point. Despite the lack of rigorous mathematical foundations, the EWT algorithm is developed based on this principle, and the successful applications of it validate its effectiveness. Inspired by this, in the ABFD method, the center frequencies are initialized at the position corresponding to the largest K maximum points of the power spectrum $|F(\omega)|^2$ to better extract the individual components.

Further explanation of the effect of variable initialization on the decomposition results will be demonstrated in conjunction with the simulation analysis in Section III.

C. THE ABFD METHOD

In the ABFD method, the core step is the separation of $\{U_k(\omega)\}$ in the frequency domain through the proposed

FSBO algorithm. According to the principle of FSBO, the decomposition results depend on the appropriate number K of BMFs. If K is too small, a sub-signal may contain too many mono-components. If K is too large, a narrowband component may be split into two or more BMFs and several redundant modes may be generated. Therefore, in order to avoid under- decomposition, K is expected to be as large as possible until the occurrence of over-decomposition. Motivated by this, an automatic detection method for K is proposed under the guidance of narrowband characteristics. The details are as follows.

Step 1: Give the initial mode number $K = 3$.

Step 2: Initialize the center frequencies at the K maximum points of the power spectrum $|F(\omega)|^2$.

Step 3: Decompose $F(\omega)$ into $\{U_k(\omega)\}$ by FSBO.

Step 4: Judge the excessive decomposition by Eq. (16). If Eq. (16) is satisfied, it indicates that at least two center frequencies are too close and a narrowband component has been excessively decomposed into several BMFs. Then, let $K = K - 1$ and end the loop; otherwise, execute Step 5.

$$\min\left(\left|\frac{\omega_{i+1}-\omega_i}{(\omega_{i+1}+\omega_i)/2}\right|\right) \le \mu \tag{16}$$

where ω_{i+1} and ω_i are two adjacent center frequencies; μ is a constant.

Step 5: Let $K = K + 1$ and go back to Step 2.

As can be seen, the number K is determined according to the distribution of center frequencies. The constant μ in Eq. (16) is the criterion for judging excessive decomposition. In ABFD method, $\mu = 0.1$, that is, excessive decomposition occurs if the superposition of two adjacent BMFs still satisfies the requirement of the narrowband characteristic [20]. Besides, K is predefined to be at least 2, which satisfies the characteristics of the multi-component signals. As for the single-component modulated signal, it can be judged according to the extreme point distribution in the frequency domain and the traditional methods can be competent for it [23].

Here, the principles and major improvements of the ABFD method have been elaborated. After $F(\omega)$ is decomposed into $\{U_k(\omega)\}$, the inverse Fourier transform is employed to convert the $\{U_k(\omega)\}$ into time-domain BMFs. For a better understanding, the flowchart of the complete ABFD for multi-component signal decomposition is presented in Fig. 1.

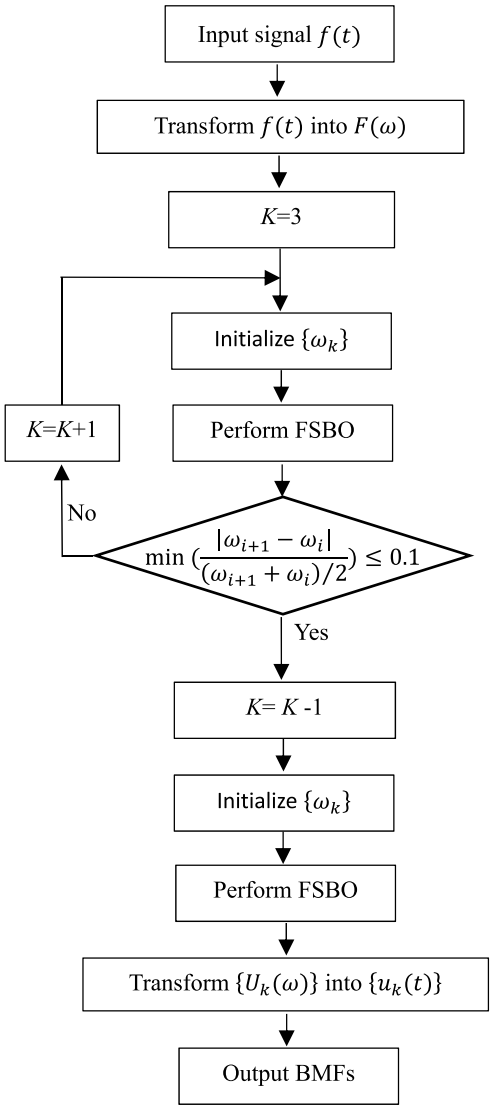

FIGURE 1. Flow chart of the proposed ABFD method.

III. SIMULATION SIGNAL ANALYSIS

In this section, some typical simulation analyses are introduced to evaluate the performance of the proposed ABFD, including decomposition capability analysis, non-stationary signal analysis, and noisy signal analysis. Meanwhile, the results are compared with those of EMD and VMD to confirm the superiority of the proposed method. In order to reduce the influence of the prior parameters in traditional VMD, the predefined mode number K and balance parameter α are optimized according to the method proposed in the literature [24]. Besides, the uniform initialization method recommended in the literature [11] is adopted to initialize the center frequencies in the VMD method.

A. THE DECOMPOSITION CAPABILITY ANALYSIS

The artificial signal f_{sig1} consisting of two pure harmonics f_{c1} and f_{c2} is under our consideration to study the decomposition capability of the algorithm:

$$f_{sig1}(t) = f_{c1} + f_{c2} = a_1\cos(2\pi v_1 f_s t) + a_2\cos(2\pi v_2 f_s t) \tag{17}$$

where a_1 and a_2 are the amplitudes of the harmonics, f_s represents the sampling frequency, v_1 and v_2 stand for the ratio of harmonic frequency to the sampling frequency. Without loss of generality, we take $f_s = 1$ and $0 < v_1, v_2 < 0.5$ according to the Shannon sampling theorem [25]. In order to quantitatively measure the decomposition capability of different methods, the relative error of the extracted high frequency harmonic is defined as the evaluation indicator:

$$e = \min\left(\|f_c(t) - u_1(t)\|_2 / \|f_c(t)\|_2,\ 1\right) \tag{18}$$

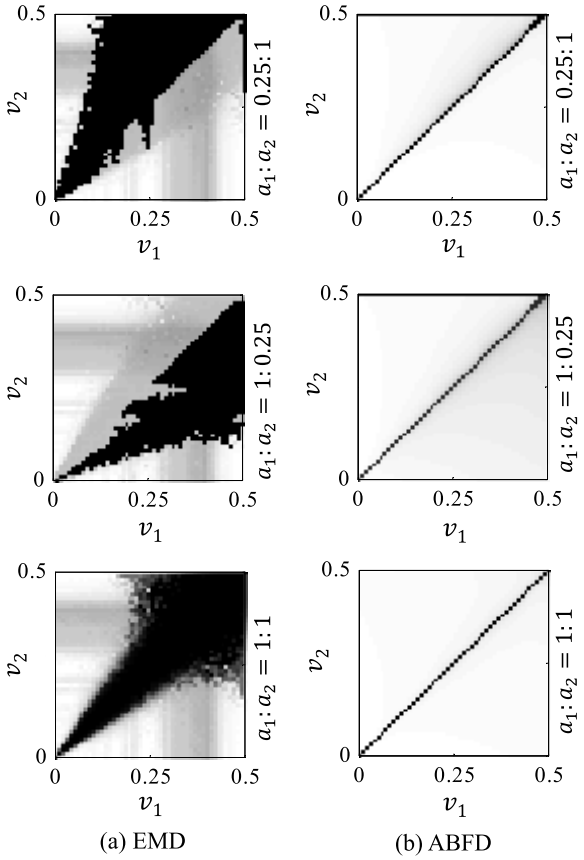

FIGURE 2. Comparisons of decomposition ability between EMD and ABFD. The plot indicates the relative error, with values between 0 (white) and 1(black). (a) Performance of EMD. (b) Performance of ABFD.

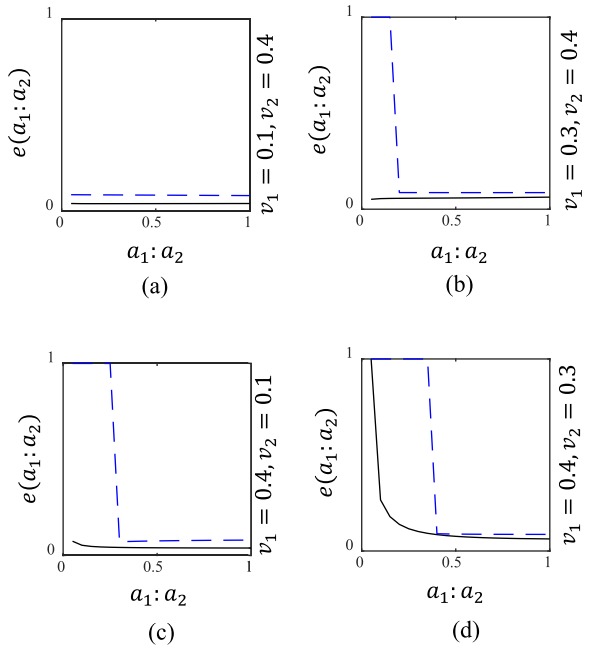

FIGURE 3. Comparisons of decomposition ability between VMD and ABFD. The black solid line is the relative error of ABFD while the blue dotted line is the relative error of VMD.

where e represents the relative error. $f_c(t)$ is the high frequency harmonic in f_{sig1} and $u_1(t)$ represents the component with the highest frequency in decomposition results. Relative error equal to zero indicates the successful recovery of high-frequency harmonic from f_{sig1} while $0 < e \leq 1$ suggests that the used signal decomposition method cannot separate two harmonics completely.

To begin with, the comparisons between EMD and ABFD at different amplitude ratios $a_1 : a_2 \in \{0.25 : 1, 1 : 0.25, 1 : 1\}$ are shown in Fig. 2, where the plot indicates the relative error, with values between 0 (white) and 1(black). The white areas represent the complete separation of the high frequency harmonic while the grey and black areas are not. It can be seen that EMD cannot separate the high-frequency harmonic when the frequencies are close. As the harmonic approaches the Nyquist frequency, the black area increases, indicating that the decomposition capability of EMD is further weakened. In contrast, ABFD shows superior performance except that the frequencies of two harmonics are almost identical.

It should be mentioned that VMD achieves good performance at different amplitude ratios $a_1 : a_2 \in \{0.25 : 1, 1 : 0.25, 1 : 1\}$ in [11]. Therefore, for further comparison, the decomposition capabilities of VMD and ABFD at different frequency ratios $v_1 : v_2 \in \{0.1 : 0.4, 0.3 : 0.4, 0.4 : 0.1, 0.4 : 0.3\}$ are studied and presented in Fig. 3. From Fig. 3(a) and Fig. 3(b), in which the low-frequency harmonic is weaker than the high-frequency harmonic, the relative error of ABFD is always close to zero, indicating the successful recovery of the high-frequency harmonic through ABFD. However, when the amplitude ratio is less than 0.15, the relative error of VMD is greater than ABFD at the frequency ratio of $0.3 : 0.4$, indicating that the signal decomposition capability of VMD is weaker than ABFD in this case. From Fig. 3(c) and Fig. 3(d), where the high-frequency harmonic is smaller than the low frequency harmonic, the relative error of ABFD is much smaller than VMD when the amplitude ratio is less than 0.35. This indicates that the proposed ABFD can better extract the weak component from the mixed signal compared with VMD.

Overall, the results in Fig. 2 and Fig. 3 demonstrate that ABFD outperforms EMD and VMD in decomposition capability. In the EMD method, the definition and judgment of IMF result in the mixed signal being treated as a mode when the harmonic components are similar. In the case of small amplitude ratio, the failure of VMD indicates that its weak component separation ability is insufficient. Since the mode number of VMD is preset to the harmonic number, it is inferred that the iterative calculation of VMD does not converge to the global optimal solution, resulting in the failure of weak component separation.

In order to further demonstrate the superiority of the proposed FSBO and the improved initialization method, the iterative process of the center frequencies in the case of frequency ratio $v_1 : v_2 = 0.4 : 0.1$ and amplitude ratio

TABLE 1. Iteration of center frequencies in the FSBO algorithm under different initialization methods.

Number of iterations	Improved initialization	Random initialization	Uniform Initialization
1	(0.40,0.10)	(0.15,0.06)	(0.25,0.00)
2	(0.40,0.10)	(0.31,0.10)	(0.30,0.10)
3		(0.40,0.10)	(0.40,0.10)
4		(0.40,0.10)	(0.40,0.10)

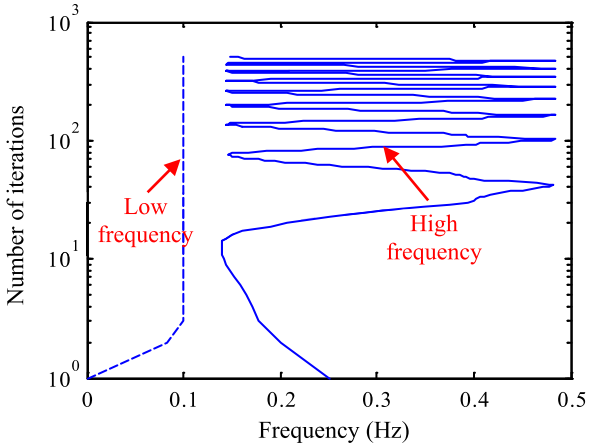

FIGURE 4. Iterative process of the center frequencies in the VMD method under uniform initialization. The solid line is the iteration of high-frequency mode and the dotted line represents the iteration of low-frequency mode.

$a_1 : a_2 = 0.1 : 1.0$ is analyzed here. It should be noted that for the sake of analysis, only the results with the determined mode number are given. The iterative process of the FSBO algorithm under different initialization methods is recorded in Table 1. For comparison, the iteration of VMD is shown in Fig. 4. As can be seen from Table 1, the improved initialization method accurately locates the harmonic frequencies and effectively reduces the number of iterations. Therefore, the improvement of the initialization method can enhance the signal separation capability of the proposed ABFD. From Fig. 4, the iteration of VMD does not converge under uniform initialization, that is, the iterative calculation is unstable in this case. However, the FSBO algorithm converges to the correct solution when the center frequencies are uniformly initialized, as shown in Table 1. Thus, it can be inferred that the bandwidth optimization algorithm of ABFD is superior to VMD in terms of stability.

B. NON-STATIONARY SIGNAL ANALYSIS

The expression of the synthetic signal f_{sig2} is given in Eq. (19), which consists of a chirp signal f_{c1} in the range of 20 to 35 Hz, an amplitude modulated harmonic f_{c2} and a segmented harmonic f_{c3}. The time sequences and Fourier spectrum of f_{sig2} sampled at 1000 Hz are depicted in Fig. 5.

$$\begin{aligned} f_{sig2} &= f_{c1} + f_{c2} + f_{c3} \\ &= chirp(0, 20, 1, 35) + e^{-2t}\sin(24\pi t) \\ &\quad + \begin{cases} 0, & t \le 0.5 \\ \sin(10\pi t), & t > 0.5 \end{cases} \end{aligned} \tag{19}$$

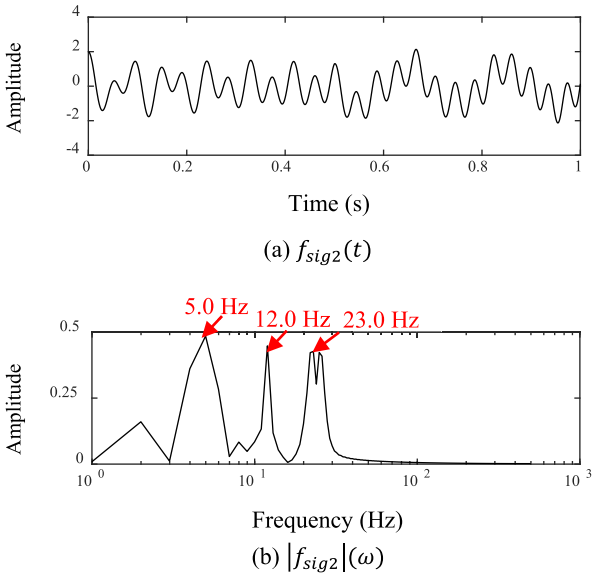

FIGURE 5. Synthetic signal f_{sig2}. (a) Time-domain waveform. (b) Fourier spectrum.

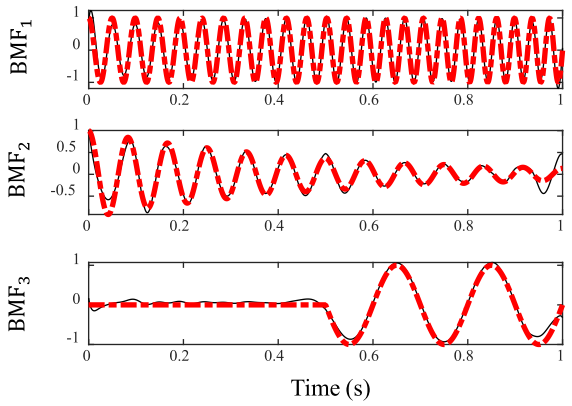

FIGURE 6. Decomposition results for f_{sig2} by ABFD. The black solid line is the decomposition result of ABFD while the red dotted line is the component of f_{sig2}.

The ABFD, EMD and VMD methods are performed on f_{sig2} and the decomposition results are illustrated in Fig. 6-8, respectively. As can be seen from Fig. 6, the original components are successfully recovered from the mixed signal by ABFD, despite a slight distortion. The sudden change of f_{c3} results in the mode mixing of EMD and a severe error in f_{c3} extraction, as presented in Fig. 7. Then the error of IMF_3 leads to the generation of several meaningless low-frequency components. The decomposition results in Fig. 8 indicate that f_{c2} and f_{c3} are mixed into one mode by VMD and a meaningless high-frequency mode is generated. Table 2 shows the iterative process of the FSBO algorithm. The iteration in VMD is exhibited in Fig. 9. The results in Table 2 suggest that the improved initialization method in ABFD can accurately locate the target frequencies and improve the convergence of the iterative calculation. From the iteration of VMD in Fig. 9,

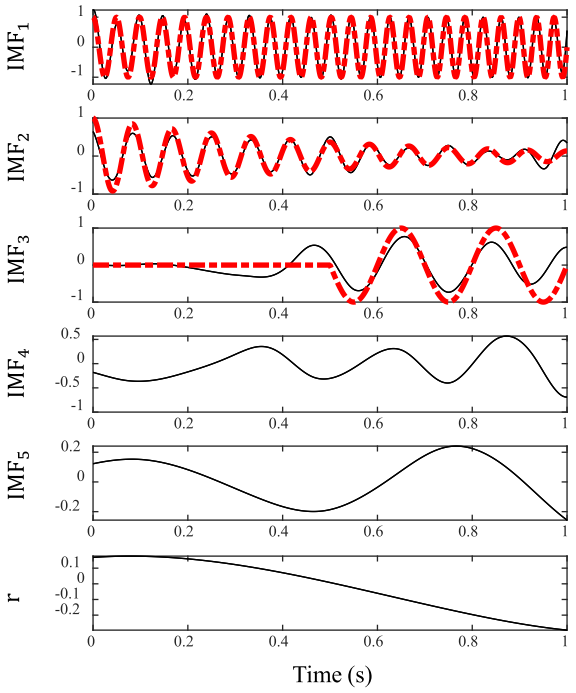

FIGURE 7. Decomposition results for f_{sig2} by EMD. The black solid line is the decomposition result of EMD while the red dotted line is the component of f_{sig2}.

TABLE 2. Iteration of the center frequencies in the FSBO algorithm.

Number of iterations	BMF_1	BMF_2	BMF_3
1	23	12	5
2	24	12	5

TABLE 3. Evaluation of the decomposition results for f_{sig2}.

Correlation coefficient	ABFD	EMD	VMD
r_1	0.991	0.991	0.992
r_2	0.962	0.948	0.507
r_3	0.993	0.776	0.867

the center frequency of IMF_1 converges to 6.4 Hz, which is between the frequencies of f_{c2} and f_{c3}. The unreasonable convergence of IMF_1 results in the mode mixing of VMD. In addition, the center frequency of IMF_3 does not converge to a certain point, which indicates that the stability of the iterative calculation in VMD is insufficient in this case.

In order to further evaluate the decomposition results, the correlation coefficient r_i between the original i-th component and the corresponding decomposition result is recorded in Table 3. In the case of mode mixing, the decomposed component most relevant to the original one is selected to computer r_i. The results in Table 3 suggest that the proposed ABFD method has significant advantages in dealing with non-stationary multicomponent signals compared to EMD and VMD.

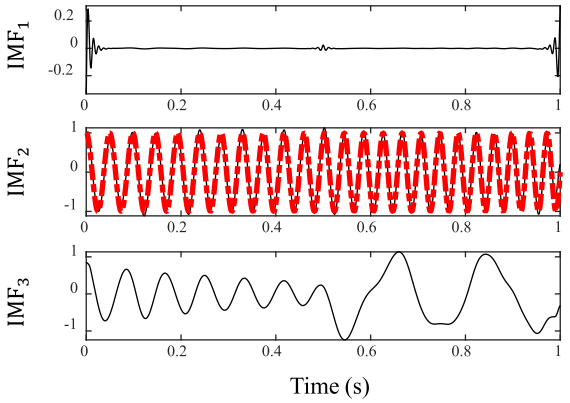

FIGURE 8. Decomposition results for f_{sig2} by VMD. The black solid line is the decomposition result of VMD while the red dotted line is the component of f_{sig2}.

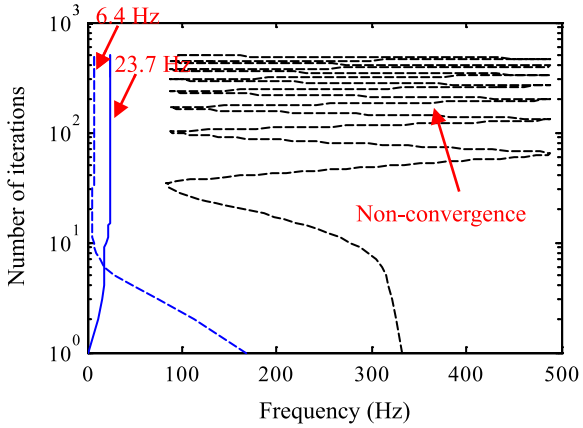

FIGURE 9. Iterative process of the center frequencies in the VMD method. The black dotted line is the iteration of IMF_1. The blue solid line represents the iteration of IMF_2. The blue dotted line denotes the iteration of IMF_3.

C. NOISY SIGNAL ANALYSIS

The noisy three-harmonic f_{sig3} presented in Eq. (20) is employed to verify the noise robustness of ABFD. The sampling frequency of the simulated signal is 2000 Hz and the time is 1.0 second.

$$f_{sig3}(t) = f_{c1} + f_{c2} + f_{c3} + \eta\frac{1}{16}\cos(576\pi t) + \frac{1}{4}\cos(48\pi t) + \cos(4\pi t) + \eta \quad (20)$$

where $\eta \sim N(0, \sigma)$ denotes the Gaussian white noise with a standard deviation of σ. Here, σ takes 0.1, which has a significant influence on the weakest harmonic as depicted in Fig. 10.

The decomposition results for f_{sig3} by ABFD are illustrated in Fig. 11. From Fig. 11(a), the strong lowest frequency harmonic is almost entirely recovered, and the medium frequency component is also reconstructed at the acceptable quality. However, the separation of the weak high-frequency harmonic is not particularly desirable due to the effect of noise. Table 4 shows the iterative process of the center

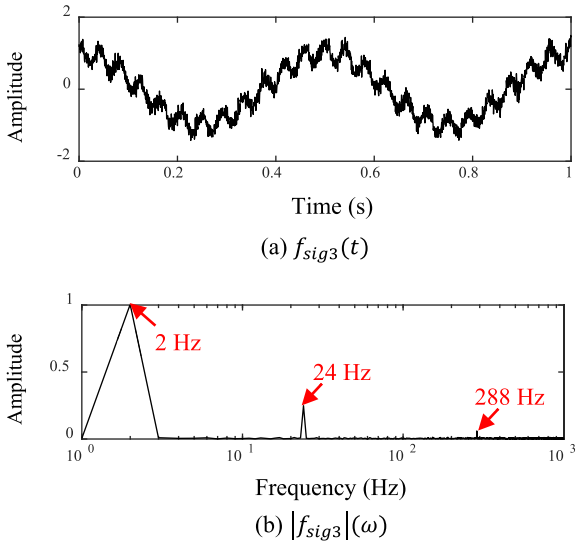

FIGURE 10. Synthetic signal f_{sig3}. (a) Time-domain waveform. (b) Fourier spectrum.

TABLE 4. Iteration of the center frequencies in the FSBO algorithm.

Number of iterations	BMF_1	BMF_2	BMF_3	BMF_4
1	797	288	24	2
2	799	329	24	2
3	800	330	24	2

frequencies. As can be seen, due to the influence of noise, the final convergence result of BMF_2 has a certain deviation from the high frequency harmonic. Nevertheless, the corresponding peak of 288 Hz can be clearly detected in the spectrum of BMF_2, as shown in Fig. 11(b).

For comparison, EMD and VMD are performed on the same data and the decomposition results are depicted in Fig. 12 and Fig. 13, respectively. As shown in Fig. 12, the high frequency harmonic is not well separated, and the medium frequency component is decomposed into the fourth, fifth and sixth modes, which can be interpreted as modal aliasing in EMD. From Fig. 13, the low and intermediate frequency harmonics are mixed into one mode in the decomposition results of VMD, which indicates that VMD does not always converge to the global optimal value in the case of noise, as demonstrated in Fig. 14. The non-convergence of center frequencies shown in Fig. 14 also reflects the insufficient stability of iterative calculation in the VMD method.

The correlation coefficients between the original harmonics and the corresponding decomposition results are recorded in Table 5. For further comparison, the average correlation coefficients of the three harmonics at different noise intensities are also presented in Table 6. In light of the results above, we can conclude that the decomposition results produced by ABFD are more related to the original harmonics and ABFD is superior to EMD and VMD in terms of noise robustness.

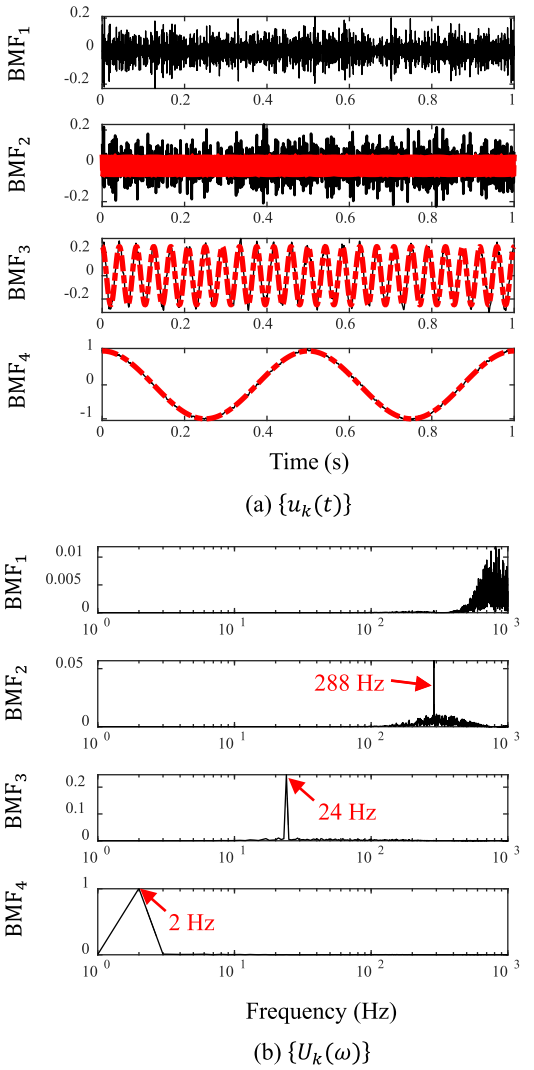

FIGURE 11. Decomposition results for f_{sig3} by ABFD. (a) Time-domain waveforms of BMFs. The black solid line is the decomposition result of ABFD while the red dotted line is the component of f_{sig3}. (b) Spectra of BMFs.

TABLE 5. Evaluation of the decomposition results for f_{sig3}.

Correlation coefficient	ABFD	EMD	VMD
r_1	0.586	0.537	0.399
r_2	0.983	0.759	0.235
r_3	1.000	1.000	0.971

In order to avoid the influence of randomness caused by Gaussian white noise, we performed the same experiments several times, and there is no essential difference in the results.

IV. MEASURED SIGNAL ANALYSIS

In this section, the effectiveness of the proposed ABFD method in practical applications is further verified by using

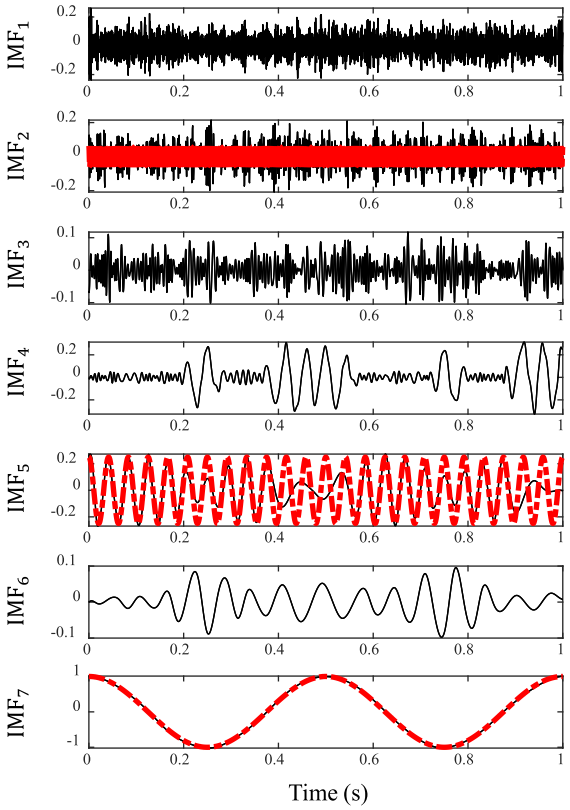

FIGURE 12. Decomposition results for f_{sig3} by EMD. The black solid line is the decomposition result while the red dotted line is the component of f_{sig3}.

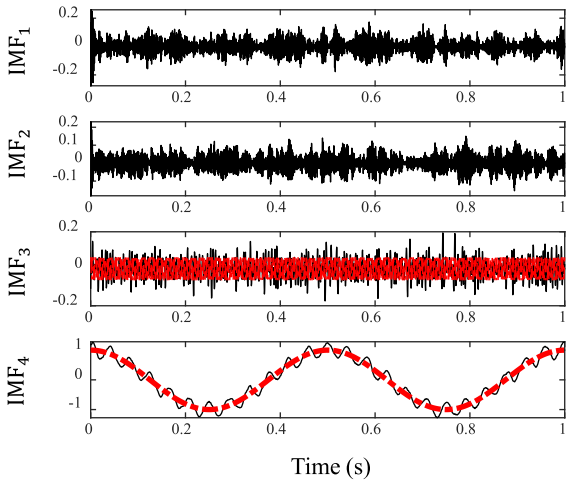

FIGURE 13. Decomposition results for f_{sig3} by VMD. The black solid line is the decomposition result while the red dotted line is the component of f_{sig3}.

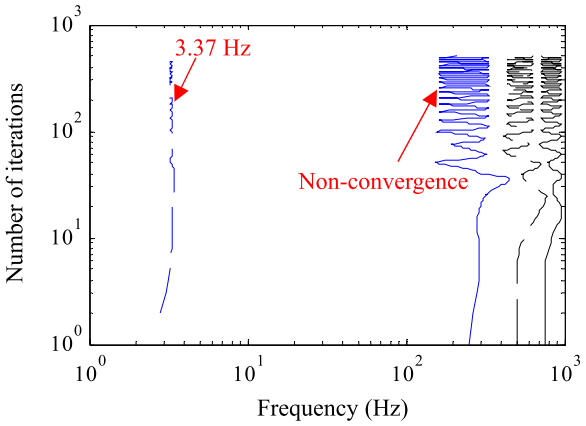

FIGURE 14. Iterative process of the center frequencies in the VMD method. The black solid line is the iteration of IMF_1. The black dotted line represents the iteration of IMF_2. The blue solid line denotes the iteration of IMF_3. The blue dotted line is the iteration of IMF_4.

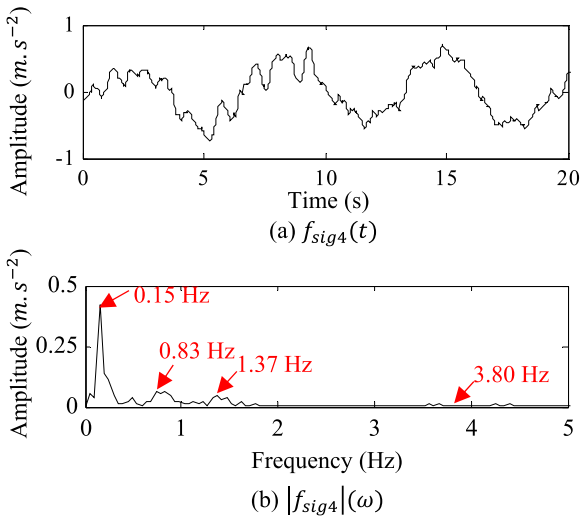

FIGURE 15. Measured vibration signal f_{sig4} of the wind turbine tower. (a) Time-domain waveform. (b) Fourier spectrum.

TABLE 6. Average correlation coefficients at different noise intensities.

Standard deviation σ	ABFD	EMD	VMD
0	1.000	1.000	0.733
0.3	0.980	0.934	0.718
0.6	0.928	0.835	0.685
0.9	0.886	0.778	0.576
1.2	0.829	0.767	0.529
1.5	0.706	0.724	0.480

two measured vibration signals. Among them, one is the vibration signal f_{sig4} of the wind turbine tower, and the other is the early fault signal f_{sig5} of the rolling bearing. Then, for comparison, the measured signals are processed using EMD and VMD.

A. TIME-FREQUENCY ANALYSIS

The vibration of the wind turbine tower is mainly induced by random wind, which makes the measured signal complex and unstable. Signal decomposition can reveal the trend of different frequency components over time, so it is a critical

TABLE 7. First four natural frequencies of the wind turbine tower.

Native mode	1	2	3	4
Natural frequency	0.15 Hz	0.83 Hz	1.37 Hz	3.80 Hz

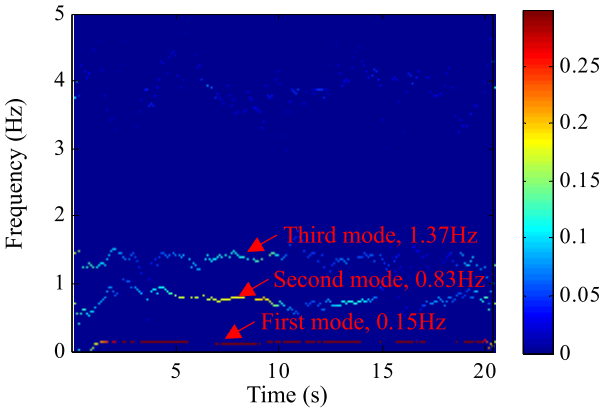

FIGURE 16. Time-frequency representation for f_{sig4} by ABFD.

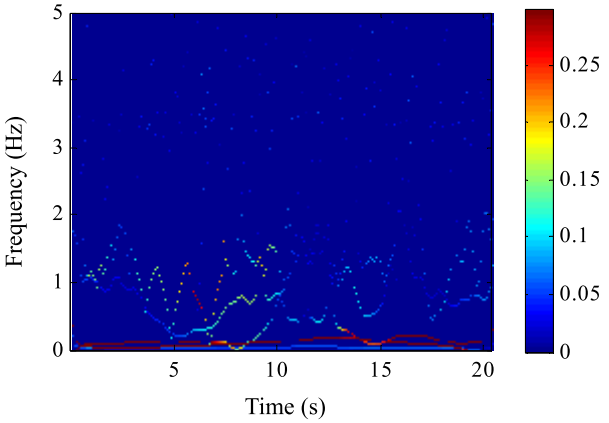

FIGURE 17. Time-frequency representation for f_{sig4} by EMD.

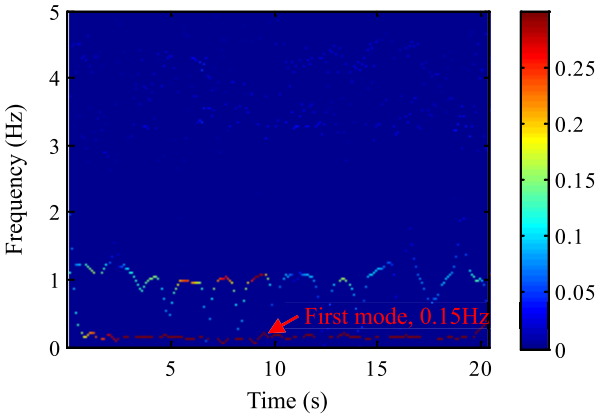

FIGURE 18. Time-frequency representation for f_{sig4} by VMD.

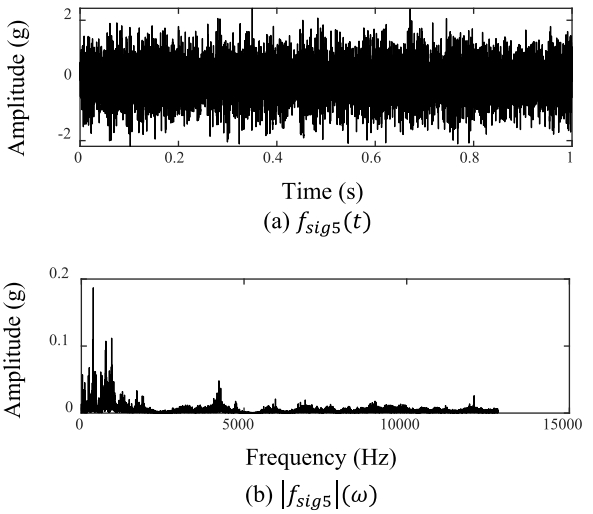

FIGURE 19. Measured rolling bearing vibration signal f_{sig5}. (a) Time-domain waveform. (b) Fourier spectrum.

step in the study of dynamic characteristics and condition monitoring of wind turbine towers.

According to the literature [26], the vibration of the wind turbine tower is a combination of different natural modes, and its natural frequency is constant. The measured first four natural frequencies of the wind turbine tower provided by the manufacturer are shown in Table 7. To collect the vibration signals, the accelerometer is mounted on the top of the wind turbine tower. The waveform and the Fourier spectrum of the vibration signal f_{sig4} sampled at 50 Hz are depicted in Fig. 15(a) and Fig. 15(b), respectively. As can be seen from Fig. 15(b), the measured vibration signal is mainly composed of the first three modes, and the fourth and higher modes can hardly be detected. Therefore, the time-frequency analysis of f_{sig4} mainly focuses on the first three modes. The first mode centered at 0.15 Hz can be observed clearly in the Fourier spectrum, while the second mode centered at 0.83 Hz and the third mode centered at 1.37 Hz are very weak. Thus, it is difficult to separate the high-order modes from the vibration signal completely.

In order to reveal the time-varying characteristics of the vibration signal clearly, the ABFD is performed on f_{sig4}, and the Hilbert transform is employed to demodulate the decomposition results to obtain the time-frequency representation. As shown in Fig. 16, the first mode is extracted completely and has a clear time-frequency representation. The separation of the second and third order modes is also acceptable although the instantaneous frequencies have a certain deviation from the natural frequencies due to the influence of noise and random interference.

Subsequently, EMD and VMD are used to process the vibration signal f_{sig4}, and the obtained time-frequency representations are shown in Fig. 17 and Fig. 18, respectively. From Fig. 17, it is difficult to recognize the different modes due to the severe mode mixing problem in EMD. In the time-frequency representation obtained by VMD,

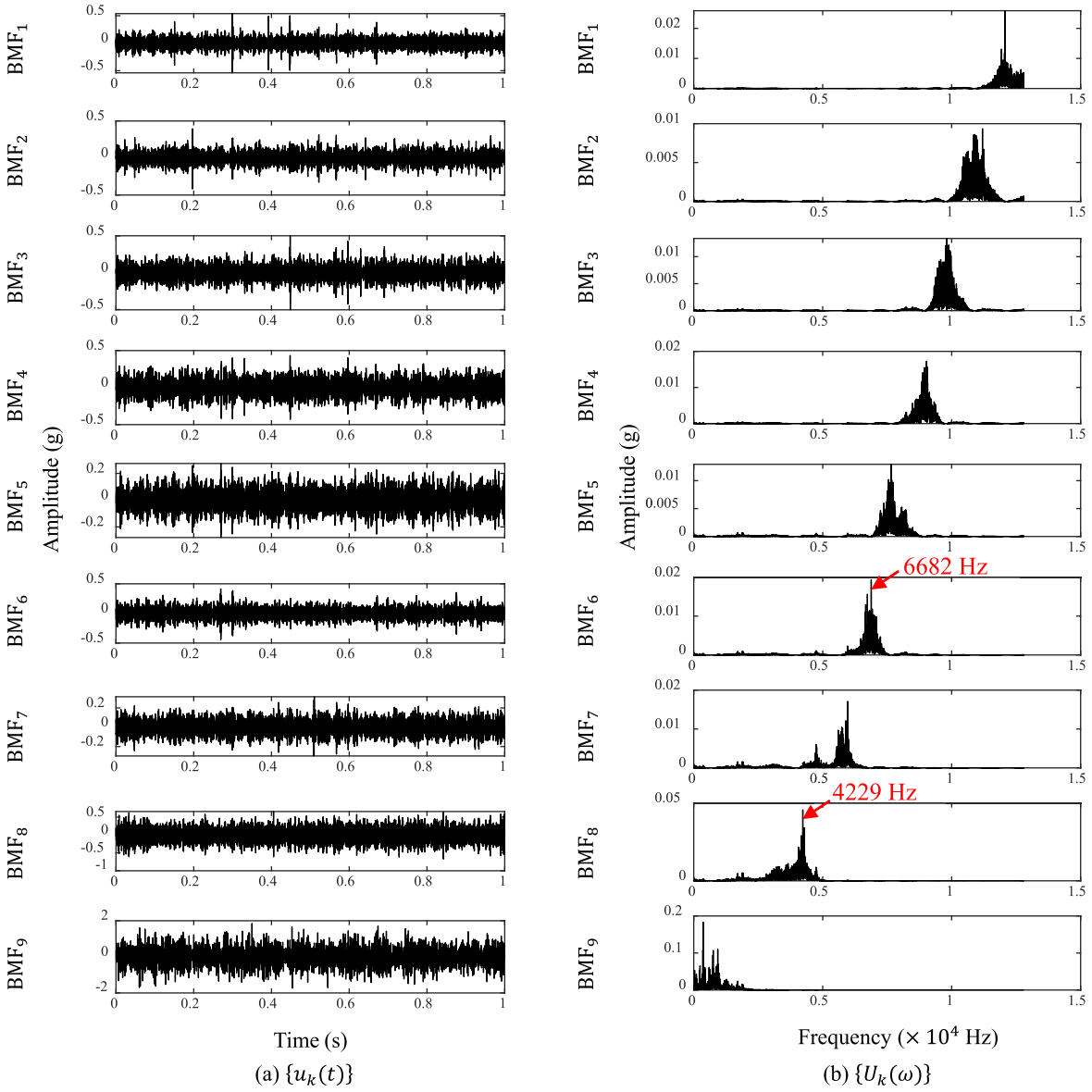

FIGURE 20. Decomposition results for f_{sig5} by ABFD. (a) Time-domain waveforms of BMFs. (b) Spectra of BMFs.

the first mode can be observed clearly. However, as shown in Fig. 18, the second and third modes are mixed into one IMF, which indicates that the VMD method has insufficient separation capability for weak components, as demonstrated in section III. Thus, from the analysis above, it is concluded that the proposed ABFD is more suitable for extracting the time-frequency characteristics of the measured signal.

B. WEAK FEATURE EXTRACTION ANALYSIS

The rolling bearing vibration signal f_{sig5} provided by the Institute of Design Science and Basic Component at Xi'an Jiaotong University is used to evaluate the performance of ABFD in extracting the weak features of the actual signal. When a local fault occurs in the rolling bearing, the characteristic signals will be modulated by the defect frequency, which can be computed according to the structure and operation parameters [27]. However, when the fault is at an early stage, the weak characteristic signals carrying the fault-related features are easily submerged in the ambient noise, making it difficult to be extracted by traditional methods.

The used vibration signal was generated by a rolling bearing with incipient outer race fault. The rotating frequency is 35 Hz, and the corresponding defect frequency is 108 Hz. For more details on the experiment and test rig, we refer to [28]. The waveform and spectrum of f_{sig5} with a sampling frequency of 25600 Hz and a sampling time of 1.0 second are drawn in Fig. 19. As can be seen, the characteristic signals have been completed contaminated by noise and no fault-related features can be observed.

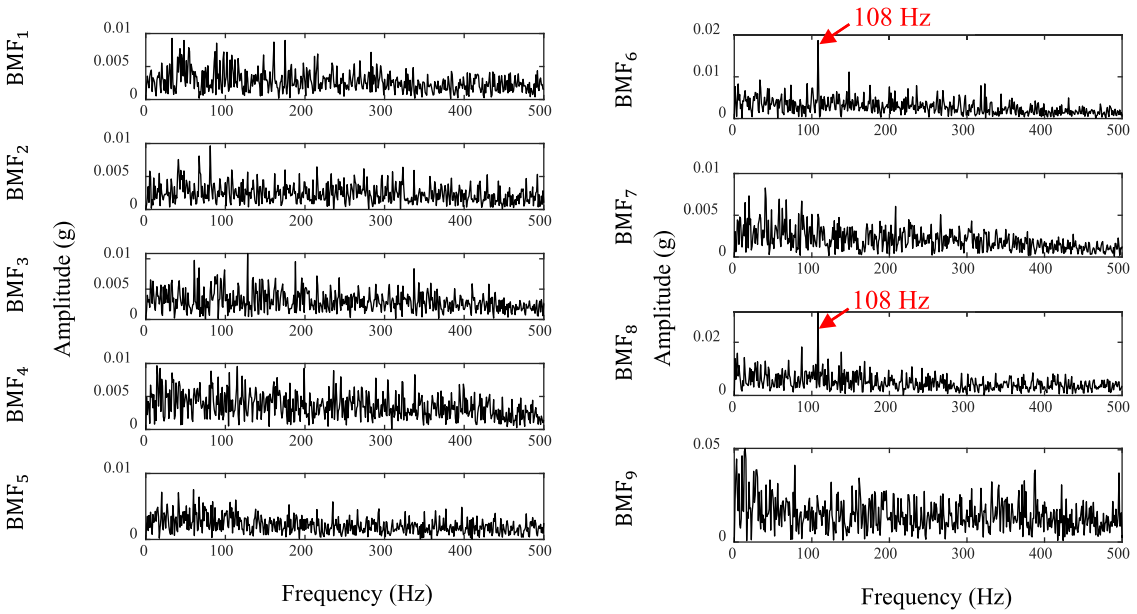

FIGURE 21. Envelope spectra obtained by ABFD.

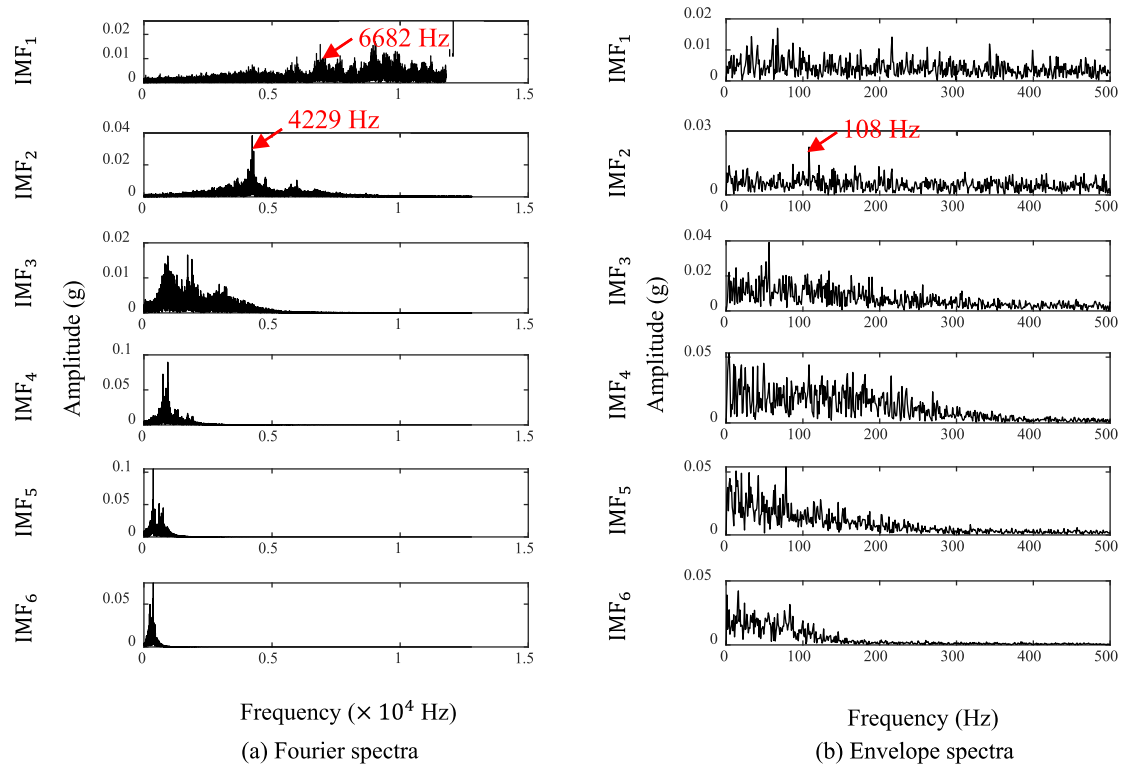

FIGURE 22. Decomposition results for f_{sig5} by EMD. (a) Fourier spectra. (b) Envelope spectra.

To begin with, the proposed ABFD method is applied to separate the characteristic signals from the original data. The waveforms and the Fourier spectra of decomposition results yielded by ABFD are illustrated in Fig. 20(a) and Fig. 20(b), respectively. Correspondingly, the envelope spectra are presented in Fig. 21. As can be seen from Fig. 21, the defect frequency of 108 Hz can be demodulated from BMF_6 and BMF_8, indicating that the fault information is carried by the characteristic signals centered at 4229 Hz and 6682 Hz.

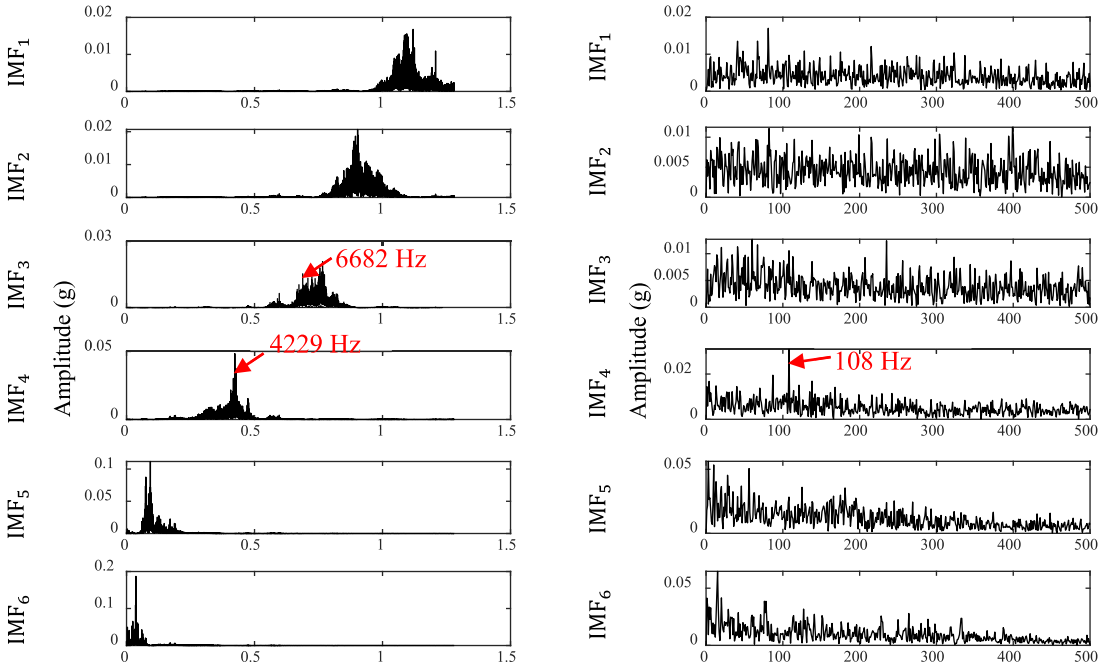

(a) Fourier spectra (b) Envelope spectra

FIGURE 23. Decomposition results for f_{sig5} by VMD. (a) Fourier spectra. (b) Envelope spectra.

Subsequently, EMD and VMD are used to extract the fault-related features hidden in original data. The Fourier spectra and the corresponding envelope spectra produced by EMD are drawn in Fig. 22(a) and Fig. 22(b), respectively. Due to the limited space, only the results of the first six IMFs containing the main feature information are presented. By observing Fig. 22(a), it can be found that the characteristic signal centered at 4229 Hz is mainly decomposed into IMF_2 by EMD and the defect frequency of 108 Hz can be detected in its envelope spectrum. However, the component centered at 6682 Hz which also carries fault-related information is mixed into IMF_1 and the defect frequency cannot be observed in its envelope spectrum due to the severe mode aliasing. From the analysis results of VMD shown in Fig. 23, the characteristic signal centered at 4229 Hz is well separated. However, the one centered at 6682 Hz is mixed into IMF_3. Due to the interference of other components in IMF_3, the defect frequency is not apparent in its envelope spectrum.

Therefore, based on the above comparison, it is concluded that ABFD can better separate the weak characteristic signals from noisy data compared with EMD and VMD.

V. COMPUTATIONAL EFFICIENCY ANALYSIS

According to the above analysis results, the capability of the proposed ABFD for multi-component signal processing is verified. Furthermore, to reflect the computational efficiency of the algorithms, the CPU running time was tested on an Intel i7-3770 3.4 GHz CPU with 16.00 GB RAM and MATLAB (R2018a) was used to run the code. In addition, the results of FSBO with predefined mode number are also listed. It is worth noting that the results of VMD are measured under predetermined parameters. Considering that the length of f_{sig1} is too short to reflect the difference between the methods, only the results of f_{sig2}, f_{sig3}, f_{sig4} and f_{sig5} are compared. From the results recorded in Table 8, the CPU running time of ABFD is significantly shorter than that of VMD due to the improvement of bandwidth optimization and variable initialization methods. Compared with EMD, the computational efficiency of the proposed ABFD needs to be further improved. The comparison between the ABFD method and the FSBO algorithm suggests that the detection process for the appropriate mode number leads to excess work, which will be further improved in our future work. Generally speaking, from the perspective of CPU running time, we can infer that the computational efficiency of ABFD

TABLE 8. Comparisons of computational efficiency using CPU time (second).

Tests	Data length	ABFD	FSBO	EMD	VMD
f_{sig2}	1000	0.163	0.057	0.162	1.778
f_{sig3}	2000	0.686	0.365	0.108	5.593
f_{sig4}	1000	0.162	0.054	0.170	1.882
f_{sig5}	25600	18.191	9.112	1.691	103.221

is satisfactory compared with VMD, although it is inferior to EMD.

VI. CONCLUSION AND DISCUSSION

In this paper, a new signal decomposition method named ABFD is proposed for multi-component signal processing. The ABFD method inherits the idea of implementing the Fourier spectrum decomposition through bandwidth optimization. In order to separate the single components more accurately, the ABFD method makes full use of the characteristics of spectral energy distribution. To evaluate the performance of the proposed ABFD, three typical artificial signals are introduced in this paper. The results indicate that the proposed ABFD outperforms EMD and VMD in decomposition capability and noise robustness, and is more suitable for non-stationary signal analysis. After that, the proposed ABFD is compared with EMD and VMD by analyzing two measured vibration signals. The analysis results show that the proposed ABFD can better extract the characteristic information from the measured signal. Finally, the comparisons of CPU running time suggest that the proposed ABFD is satisfactory in computational efficiency. The major contributions and conclusions of this paper are summarized as follows:

1) The proposed ABFD is developed based on the bandwidth optimization. In order to reduce the computational complexity, a novel bandwidth optimization algorithm termed FSBO is proposed in this paper. The analysis results show that compared with VMD, the iterative calculation of FSBO converges faster and is more stable.

2) We also notice the effect of variable initialization on the convergence of the iterative calculation. Inspired by the EWT method, a novel variable initialization method based on the spectral energy distribution is proposed to better separate the narrowband AM-FM components.

3) Under the guidance of narrowband characteristics, a method for automatically determining the appropriate mode number is proposed. The excellent performance of ABFD verifies its effectiveness. However, this approach increases the computational effort, which will be further improved in our future work.

REFERENCES

[1] P. Singh, S. D. Joshi, R. K. Patney, and K. Saha, "The Fourier decomposition method for nonlinear and non-stationary time series analysis," *Proc. Roy. Soc. A, Math., Phys. Eng. Sci.*, vol. 473, no. 2199, Mar. 2017, Art. no. 20160871.

[2] X. Yan, M. Jia, W. Zhang, and L. Zhu, "Fault diagnosis of rolling element bearing using a new optimal scale morphology analysis method," *ISA Trans.*, vol. 73, pp. 165–180, Feb. 2018.

[3] Y. Xin, Y. Chen, and W. T. Hao, "ECG baseline wander correction based on mean-median filter and empirical mode decomposition," *Bio-Med. Mater. Eng.*, vol. 24, no. 1, pp. 365–371, 2014.

[4] Q. Chen, N. E. Huang, S. Riemenschneider, and Y. Wu, "A B-spline approach for empirical mode decompositions," *Adv. Comput. Math.*, vol. 24, nos. 1–4, pp. 171–195, Jan. 2006.

[5] J. Zheng, H. Pan, T. Liu, and Q. Liu, "Extreme-point weighted mode decomposition," *Signal Process.*, vol. 142, pp. 366–374, Jan. 2018.

[6] H. Liu, X. Wang, and C. Lu, "Rolling bearing fault diagnosis based on LCD–TEO and multifractal detrended fluctuation analysis," *Mech. Syst. Signal Process.*, vols. 60–61, pp. 273–288, Aug. 2015.

[7] Z. Haiyang, W. Jindong, J. Lee, and L. Ying, "A compound interpolation envelope local mean decomposition and its application for fault diagnosis of reciprocating compressors," *Mech. Syst. Signal Process.*, vol. 110, pp. 273–295, Sep. 2018.

[8] L. Wang, Z. Liu, Q. Miao, and X. Zhang, "Complete ensemble local mean decomposition with adaptive noise and its application to fault diagnosis for rolling bearings," *Mech. Syst. Signal Process.*, vol. 106, pp. 24–39, Jun. 2018.

[9] J. Gilles, "Empirical wavelet transform," *IEEE Trans. Signal Process.*, vol. 61, no. 16, pp. 3999–4010, Aug. 2013.

[10] Y. Hu, F. Li, H. Li, and C. Liu, "An enhanced empirical wavelet transform for noisy and non-stationary signal processing," *Digit. Signal Process.*, vol. 60, pp. 220–229, Jan. 2017.

[11] K. Dragomiretskiy and D. Zosso, "Variational mode decomposition," *IEEE Trans. Signal Process.*, vol. 62, no. 3, pp. 531–544, Feb. 2014.

[12] F. Li, R. Li, L. Tian, L. Chen, and J. Liu, "Data-driven time-frequency analysis method based on variational mode decomposition and its application to gear fault diagnosis in variable working conditions," *Mech. Syst. Signal Process.*, vol. 116, pp. 462–479, Feb. 2019.

[13] X. Bi, S. Cao, and D. Zhang, "A variety of engine faults detection based on optimized variational mode decomposition-robust independent component analysis and fuzzy c-mean clustering," *IEEE Access*, vol. 7, pp. 27756–27768, 2019.

[14] X. Wang, W. Fan, X. Li, and L. Wang, "Weak degradation characteristics analysis of UAV motors based on Laplacian Eigenmaps and variational mode decomposition," *Sensors*, vol. 19, no. 3, p. 524, Feb. 2019.

[15] X. Jiang, J. Wang, J. Shi, C. Shen, W. Huang, and Z. Zhu, "A coarse-to-fine decomposing strategy of VMD for extraction of weak repetitive transients in fault diagnosis of rotating machines," *Mech. Syst. Signal Process.*, vol. 116, pp. 668–692, Feb. 2019.

[16] B. Xu, F. Zhou, H. Li, B. Yan, and Y. Liu, "Early fault feature extraction of bearings based on Teager energy operator and optimal VMD," *ISA Trans.*, vol. 86, pp. 249–265, Mar. 2019.

[17] D. Wei, H. Jiang, H. Shao, X. Li, and Y. Lin, "An optimal variational mode decomposition for rolling bearing fault feature extraction," *Meas. Sci. Technol.*, vol. 30, no. 5, May 2019, Art. no. 055004.

[18] G. Z. Li, G. Tang, G. G. Luo, and H. Wang, "Underdetermined blind separation of bearing faults in hyperplane space with variational mode decomposition," *Mech. Syst. Signal Process.*, vol. 120, pp. 83–97, Apr. 2019.

[19] J. Ma, J. Wu, and X. Wang, "Incipient fault feature extraction of rolling bearings based on the MVMD and Teager energy operator," *ISA Trans.*, vol. 80, pp. 297–311, Sep. 2018.

[20] J. Lian, Z. Liu, H. Wang, and X. Dong, "Adaptive variational mode decomposition method for signal processing based on mode characteristic," *Mech. Syst. Signal Process.*, vol. 107, pp. 53–77, Jul. 2018.

[21] X. Jiang, C. Shen, J. Shi, and Z. Zhu, "Initial center frequency-guided VMD for fault diagnosis of rotating machines," *J. Sound Vib.*, vol. 435, pp. 36–55, Nov. 2018.

[22] Y. Li, M. Xu, X. Liang, and W. Huang, "Application of bandwidth EMD and adaptive multiscale morphology analysis for incipient fault diagnosis of rolling bearings," *IEEE Trans. Ind. Electron.*, vol. 64, no. 8, pp. 6506–6517, Aug. 2017.

[23] A. Chen and T. R. Kurfess, "Signal processing techniques for rolling element bearing spall size estimation," *Mech. Syst. Signal Process.*, vol. 117, pp. 16–32, Feb. 2019.

[24] X. Jiang, S. Li, and C. Cheng, "A novel method for adaptive multiresonance bands detection based on VMD and using MTEO to enhance rolling element bearing fault diagnosis," *Shock Vib.*, vol. 2016, Aug. 2016, Art. no. 8361289.

[25] A. Bhandari and Y. C. Eldar, "Sampling and super resolution of sparse signals beyond the Fourier domain," *IEEE Trans. Signal Process.*, vol. 67, no. 6, pp. 1508–1521, Mar. 2019.

[26] C. Cong, "Using active tuned mass dampers with constrained stroke to simultaneously control vibrations in wind turbine blades and tower," *Adv. Struct. Eng.*, vol. 22, no. 7, pp. 1544–1553, May 2019.

[27] K. J. Moore, M. Kurt, M. Eriten, D. M. McFarland, L. A. Bergman, and A. F. Vakakis, "Wavelet-bounded empirical mode decomposition for vibro-impact analysis," *Nonlinear Dyn.*, vol. 93, no. 3, pp. 1559–1577, Aug. 2018.

[28] B. Wang, Y. Lei, N. Li, and N. Li, "A hybrid prognostics approach for estimating remaining useful life of rolling element bearings," *IEEE Trans. Rel.*, to be published.

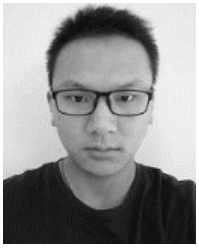

MINQIANG DENG received the M.S. degree from Southeast University, Nanjing, China, where he is currently pursuing the Ph.D. degree in engineering. His current research interests include signal processing, machine learning, and fault diagnosis.

AIDONG DENG received the Ph.D. degree in engineering from Southeast University, Nanjing, China, where he is currently a Professor and a Doctoral Advisor. His current research interests include signal processing, machine learning, and mechanism analysis.

JING ZHU received the M.S. degree from Southeast University, Nanjing, China, where she is currently pursuing the Ph.D. degree in engineering. Her current research interests include signal processing, machine learning, and vibration control.

WENQING SUN received the B.S. degree from Soochow University, Suzhou, China. He is currently pursuing the M.S. degree in engineering with Southeast University, Nanjing, China. His current research interests include deep learning and artificial intelligence.